VOL. 10, NO 19, OCTOBER, 2015 ISSN 1819-6608
ARPN Journal of Engineering and Applied Sciences

www.arpnjournals.com

OPTIMAL TORQUE INVESTIGATION OF OUTER-ROTOR HYBRID EXCITATION FLUX SWITCHING MACHINE FOR IN-WHEEL DRIVE EV

M. Z. Ahmad[1,2], E. Sulaiman[1,2], G. M. Romalan[1,2], and Z. A. Haron[1]
[1]Faculty of Electrical and Electronic Engineering, UTHM, Johor, Malaysia
[2]Research Center for Applied Electromagnetics, UTHM, Johor, Malaysia
E-Mail: zarafi@uthm.edu.my

ABSTRACT

This paper present an optimal torque investigation of outer-rotor hybrid excitation flux switching machine (OR-HEFSM) for in-wheel drive electric vehicle (EV). Previously, most of the successful electric machines for electric drive in EV/HEV is interior permanent magnet synchronous motor (IPMSM) due to their ability to deliver high torque and power densities for great starting and climbing conditions. Nevertheless, the IPMSM has some demerit owing to high volume of permanent magnet (PM) used and unrobustness rotor. As an alternative candidates, flux switching machine (FSM) having robust rotor structure and higher torque capability has been proposed for EV/HEV drive and many research has been reported over the last decade. However, most of them are mainly focused on inner-rotor configuration. Therefore, in this paper the proposed OR-HEFSM is investigated to have maximum performances similar to IPMSM conventionally employed in existing HEV. Several defined parameters of OR-HEFSM are treated using deterministic optimization method to attempt maximum torque performance. After several cycles of optimization investigation, the proposed machine has achieved the target maximum average torque and power of 335.08Nm and 160.2kW, respectively.

Keywords: permanent magnet, hybrid excitation coil, outer-rotor, in-wheel, electric vehicle.

INTRODUCTION

Electric vehicles (EVs) and hybrid electric vehicles (HEVs) have attracted increasing attentions in reducing emissions and improving fuel economy, (Chan, 2007). The motors for drive system are expected to have high reliability, large torque and power densities, and enough overload capabilities. Flux-switching machines (FSMs) is an alternative candidates that have attracted considerable interests for high performance drive applications due to the high torque and power densities (Yan *et al.*, 2013, Sulaiman, Kosaka, and Matsui, 2011, Xu *et al*., 2009). In addition, since all active components are accommodated on the stator body making the FSMs have simple and robust rotor structure and appropriates for high-speed applications (Ahmad, 2013).

Nevertheless, to date most of published report of FSMs on design and improvement are only focused on inner-rotor configuration (Pollock and Brackley, 2003), (Xu *et al.,* 2010), (Chen and Zhu, 2010), (Wang and Deng, 2012), (Tang *et al*., 2012), (E. Sulaiman, T. Kosaka, and N Matsui, 2010, 2014). Lately, several report have discussed on outer-rotor FSM configuration which employed only PM or field wound (FW) as a main flux source. The proposed motors specially designed to be applied for in-wheel light EV and aerospace application (Fei *et al*., 2012), (Galea, Gerada, and Hamiti, 2012). Some drawback has been identified on both motors which is uncontrollable flux and segmented rotor for PMFSM and FWFSM, respectively. This may contributes to difficulty control in flux weakening region and less robust of rotor structure, correspondingly. Thus, this paper proposed a new structure of outer-rotor FSM with hybrid excitation coil having single stacked stator iron core and salient rotor. Hence, the additional field excitation (FE) coil has provided flux control capability that beneficial in flux weakening operation, while the salient rotor structure has contributed on robustness. The machine inherits combination advantages of permanent magnet synchronous motor (PMSM) and switched-reluctance motor (SRM) (A. Shakila Banu and Wahidabanu RSD, 2014). The study has focused on optimal torque investigation to meet the target torque and power performances for in-wheel drive EV application. The design specifications are based on the successfully developed interior permanent magnet synchronous machine (IPMSM) installed in Lexus Toyota RX400h. The original structure of the proposed machine is illustrated in Figure-1. The proposed machine has 12 PMs and 12 FE coils which spread uniformly in the middle of each armature coil. The three-phase armature coils are put in the 12 slots on each quarter of stator body periodically.

DESIGN SPECIFICATIONS

The design specifications of the machine is summarized in Table-1. The specifications have been chosen based on the successful IPMSM employed in

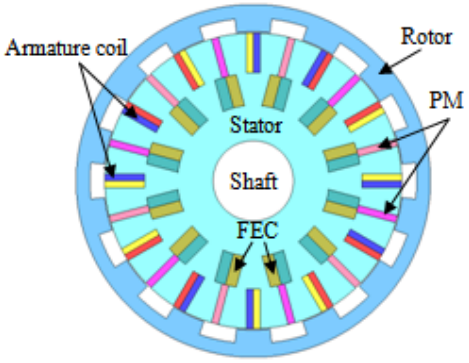

Figure-1. Cross sectional view of original 12S-14P outer-rotor HEFSM.

Table-1. The outer-rotor design constraints.

Descriptions	IPMSM	Outer-rotor HEFSM
Max. DC-bus voltage inverter (V)	650	650
Max. inverter current (A_{rms})	360	360
Max. J_a (A_{rms}/mm^2)	Conf.	30
Max. J_e (A/mm^2)	NA	30
Motor radius (mm)	132	132
Motor stack length (mm)	70	70
Shaft/Inner motor radius (mm)	30	30
Air gap length (mm)	0.8	0.8
PM weight (kg)	1.1	1.0
Total weight (kg)	35	<30
Maximum torque (Nm)	333	>333
Maximum power (kW)	123	>123

existing HEV. All dimensions of the proposed machine are kept similar as IPMSM but the PM weight is reduced into 1.0kg. The target maximum average torque and power is also expected can achieve at least 333Nm and 123kW, respectively. Furthermore, with the inverter rating of 650V/350Arms, both armature current and DC FEC current densities are set at 30 A_{rms}/mm^2 and 30 A/mm^2, respectively. By expecting the total weight of the machine is less than 35kg, therefore the proposed machine will have maximum torque and power densities greater than 9.51Nm/kg and 3.51kW/kg, respectively. The current density of armature coil and DC FEC can be examined by equation (1) and equation (2), respectively.

$$J_a = \frac{I_a N_a}{\alpha_a S_a} \quad (1)$$

$$J_e = \frac{I_e N_e}{\alpha_e S_e} \quad (2)$$

where, I_a is the rms current of armature coil and N_a is the armature coil turns, while α_a and S_a is the filling factor and armature coil slot area, respectively. On the other hand, superscript 'e' in equation (2) is indicates to FEC components. Whilst, the number of turns of armature coil and FEC is calculated by equation (3) and (4).

$$N_a = \sqrt{\frac{\alpha_a R_a S_a}{4\rho L_{a-ave}}} \quad (3)$$

$$N_e = \sqrt{\frac{\alpha_e R_e S_e}{4\rho L_{e-ave}}} \quad (4)$$

where, , R is the coil resistance (Ω), S is the coil slot area (mm^2), and L is the average coil length (mm). Hence, the designed parameters of N_a, N_e, J_a and J_e, of the original design machine are listed in Table 2.

DESIGN PARAMETERS OPTIMIZATION

Based on the calculated torque and power of initial design machine, the performances are still far from the target which only can achieved 243.52Nm and 83.03kW, respectively, which still far from the target performances. In order to meet the target performances, some design improvement and optimization has been conducted using deterministic optimization method. The parameters related to rotor and stator are depicted in Figure-2, which are inner rotor radius (L_1), rotor pole depth (L_2), rotor pole width (L_3), PM depth (L_4) and PM width (L_5). Besides, the parameters associated with the winding slot are FEC slot depth (L_6), FEC slot width (L_7), armature slot depth (L_8) and armature slot width (L_9). Finally, the gap between the upper edge of stator tooth and PM is marked by (L_{10}) and air gap length is set at 0.8mm for the whole optimization process.

Table-2. Original machine's parameter specifications.

Armature		Excitation	
α_a	**0.6**	α_e	**0.6**
R_a	1 Ω	R_e	1 Ω
S_a	147.08 mm^2	S_e	197.51mm^2
ρ	1.673E-08 Ωm	ρ	1.673E-08 Ωm
N_a	7turns	N_e	44turns
J_a	30A/mm^2	J_e	30A/mm^2

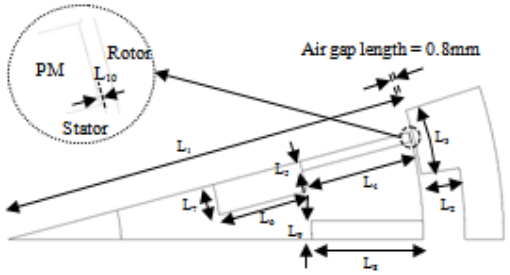

Figure-2. Defined parameters for optimization.

Firstly, the most dominant parameter of L_1 is varying to attempt the optimal torque while keeping the other parameters constant. The torque at various point of L_1 is plotted in Figure-3 and maximum torque has been obtained when L_1 is set at 113.4mm. By keeping this parameter, then the parameters of L_2 and L_3 are changed and the results obtained are shown in Figure-4. The graph shows that the optimal torque has been examined when L_2 and L_3 is set at 9.3 mm and 7.43 mm, respectively.

Secondly, the parameters related to PM which is L_4 and L_5 are adjusted by considering the PM is the main flux source. Throughout the optimization of PM's parameters, the PM area is remained constant to has 1.0kg PM weight.

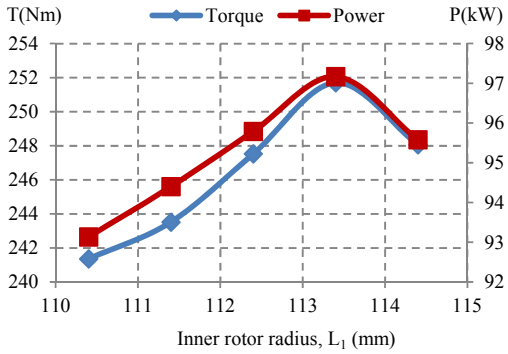

Figure-3. Torque at various inner rotor radius, L_1.

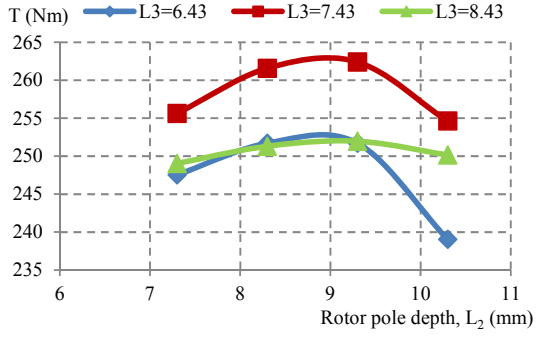

Figure-4. Torque versus rotor pole depth, L_2 at various rotor pole width, L_3.

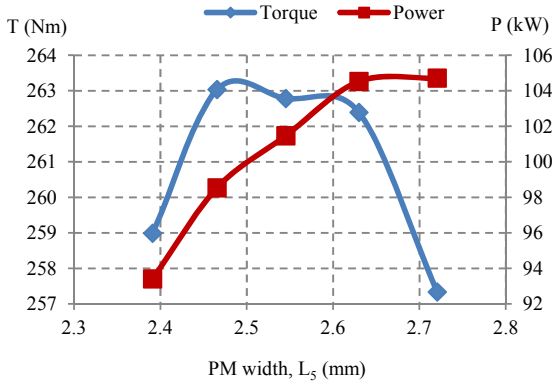

Figure-5. Torque and power versus PM width, L_5 at various PM depth, L_4.

Figure-5 demonstrates the change of torque and power when parameter L_4 and L_5 is adjusted. The analysis is done at five points which marked by No. 1(L_4=33mm), No. 2 (L_4=32mm), No. 3 (L_4=31mm), No.4 (L_4=30mm), and No. 5 (L_4= 29mm). The maximum torque was obtained when L_5 is set at 32mm and 2.47mm, respectively. On the other hand, the maximum power is obtained when L_4 is set at 29 mm and L_5 is set at 2.72 mm. Since, the torque performance is still far from the target; therefore point No. 2 is selected as the optimal point and proceeds to further improve for the next parameter.

Furthermore, with the parameter of L_4 and L_5 that bring optimal torque, parameter L_6 and L_7 of FEC slot is then adjusted and kept the other parameters constant. Torque and power at various depth and width of FEC slot are plotted in Figure 6. Based on the demonstrated graph, the best combination torque and power is when L_6 and L_7 is set at 19.88 mm and 8.25 mm, respectively.

The armature coil slot parameters of L_8 and L_9 are also adjusted to find the optimal torque. Similar as previous steps, the other parameters are kept constant when treating a particular parameter. The armature coil slot area is remained constant and analysis is completed at five point of armature coil slot width, L_9 labelled by No. 1 (8.36mm), No. 2 (7.82mm), No. 3 (7.34mm), No. 4 (6.92mm), and No. 5 (6.54mm) as depicted in Figure-7. From the graph, the optimal torque has been obtained at point No. 3 then selected as the best parameters to be used. The effect on the armature winding turns are also investigated. The torque versus number of turn of armature coil is shown in Figure-8. Based on the graph, 6 turns of armature winding is the best which can deliver optimal torque performance. Finally, to ensure the machine can deliver better performances, both FEC and armature coil slots are into trapezoidal shape to allow maximum flux flow through their path easily. Then, some of FEC and armature coil slot edge is redesigned to have curve shape in order to provide optimal performances. Each of

parameter is treated repeatedly until the target torque and power are achieved. Through numerous optimization cycles, the target torque and power of 333Nm and 123kW are realized as demonstrated in Figure-9. The final design machine shown in Figure-10 has better performances compared to the IPMSM.

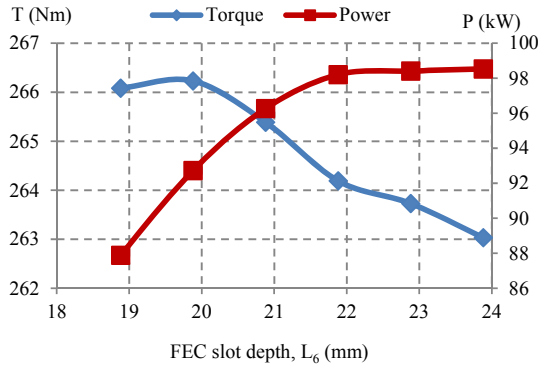

(a) Torque and power versus FEC slot depth, L_6

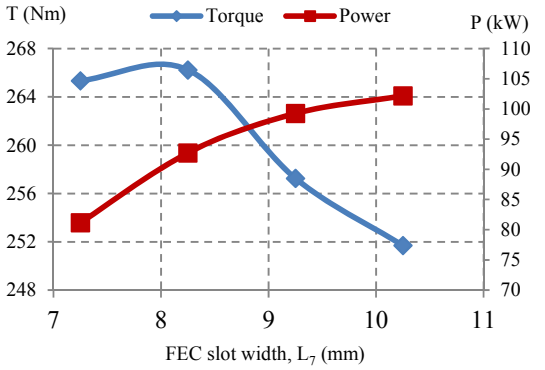

(b) Torque and power versus FEC slot width, L_7

Figure-6. Torque and power at various L_6 and L_7 of FEC slot parameters.

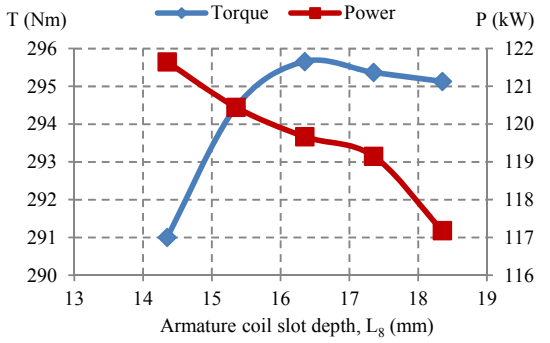

Figure-7. Torque and power at various armature coil slot depth, L_8.

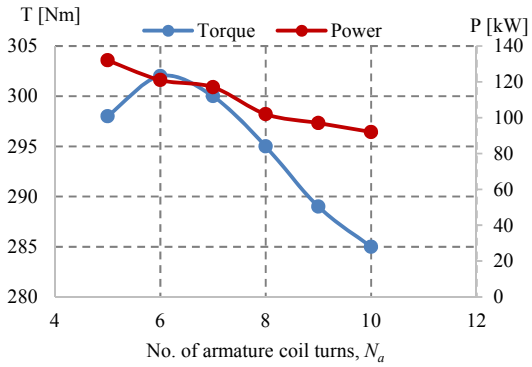

Figure-8. Torque and power at various N_a.

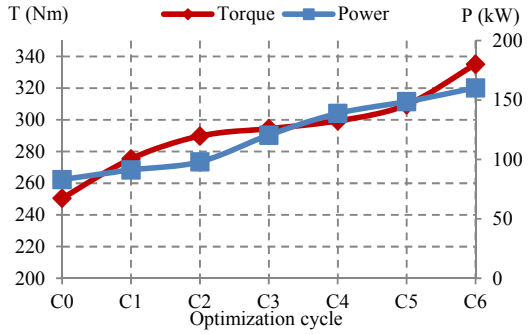

Figure-9. Several cycles of optimization process.

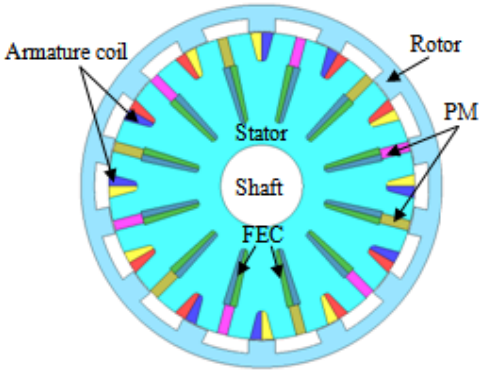

Figure-10. Optimized design structure.

RESULTS AND DISCUSSIONS

No-load analysis

Several analysis at no load analysis have been conducted to monitor and compare the machine's performances. Initially, back-emf of original and final design machine at speed of 3000r/min is evaluated and plotted in Figure-11. The amplitude of back-emf of final design machine is lower than the initial design machine with the different of approximately 17Nm. In addition, the amplitude of cogging torque of final design machine has reduced dramatically from approximately 4.1Nm (peak) to 0.2Nm (peak) of final design as shown in Figure-12.

Torque versus current densities

In load analysis, both armature coil and FEC current densities is varied from 0 A/mm^2 to 30A/mm^2. Figure-13 illustrates the torque performance at various current densities. Based on d-q coordinate transformation, and assuming the d-axis current controlled to zero while voltage drop at armature resistance is negligible when compared to the back-emf, the torque is calculated as in (5).

$$T = \left[(\phi_m + \phi_e) i_q \right] \quad (5)$$

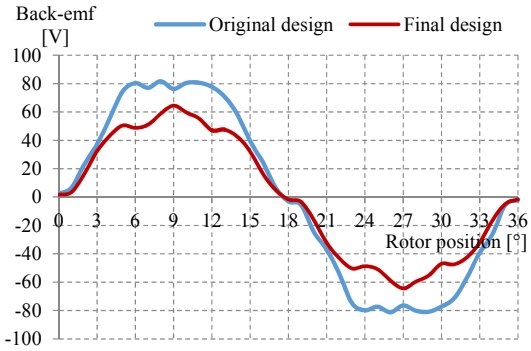

Figure-11. Back-emf.

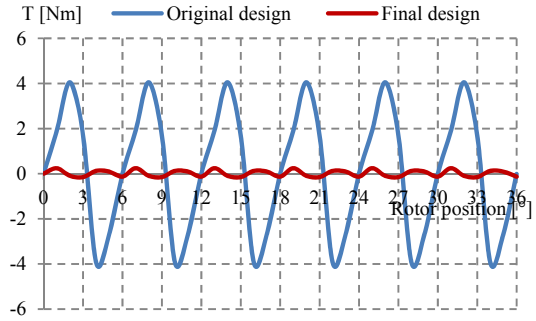

Figure-12. Cogging torque.

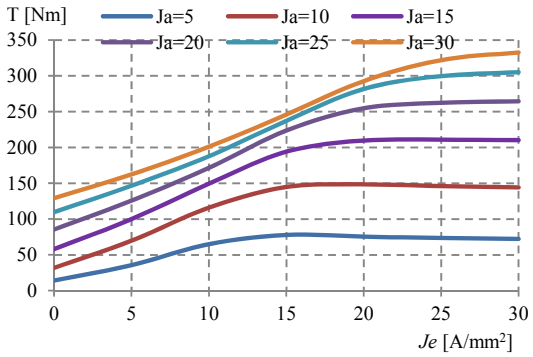

Figure-13. Torque versus FEC current density at various armature current density.

where P_n is the number of pole-pair, ϕ_m is the PM flux linkage, and ϕ_e is the flux linkage produced by mmf of excitation coil. According to Figure-15, an increase in armature current density will increase the torque and the maximum torque has been obtained when J_a and J_e are set at maximum of 30A/mm^2.

Torque and power characteristics

The torque and power characteristics is plotted in Figure-14. The final design machine has wide constant maximum torque of 335.08Nm with the base speed of 4,149r/min, while the maximum power of 160.2kW has been achieved. With the calculated weight of 27.03kg which includes copper and PM weight, the final design machine has reached maximum torque and power densities of 12.4Nm/kg and 5.9kW/kg, respectively.

Mechanical stress analysis

The centrifugal force analysis is also has been conducted based on 2D FEA to analyse the rotor mechanical strength performance. The analysis is done at maximum speed of 12,400r/min and it is obvious that the maximum principle stress is only 377.29Mpa as shown in Figure 15 and still less than the maximum allowable mechanical stress of the material used which is 481Mpa. Therefore, the mechanical strength of the electromagnetic steel 35H210 used in this analysis is within the acceptable range.

Machine loss and efficiency

Based on FEA, the proposed machine losses and efficiency are examined. Copper loss on each winding and iron loss on the stator and rotor core is also took into consideration. The machine losses and efficiency at several motor operating conditions are calculated and the results are illustrated in Figure-16 and Figure-17, respectively. The operating point at base speed, maximum speed and frequent driving conditions labelled by No. 1 to No. 8 in Figure 14 are evaluated. It is obvious that, from Figure 16 the highest output power is generated at point

No. 2 with has been reached approximately 159.32kW. However, iron loss at this point is the highest with the amount of 44.5kW. This is expected the machine with outer-rotor configuration has led to higher iron loss of rotor compared with inner rotor configuration.

Furthermore, the calculated efficiency of the machine has shows that the highest efficiency has been obtained at low speed of normal driving condition labelled by point No. 3 and No. 6, which almost reached 95%. At high speed conditions such as at point No. 2, No. 5, and No. 8, the efficiency have much degraded which mostly are not more than 85%. Nonetheless, the average efficiency at normal driving conditions is approximately 88%, which can be considered within the acceptable range for in-wheel drive application.

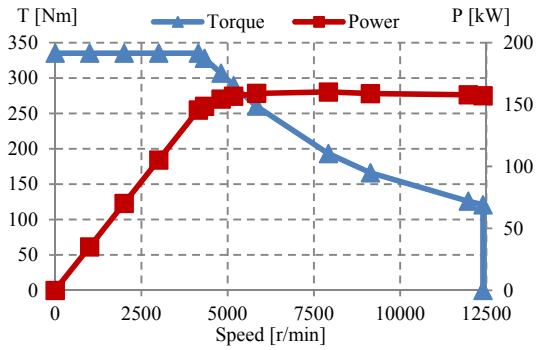

Figure-14. Torque and power characteristics.

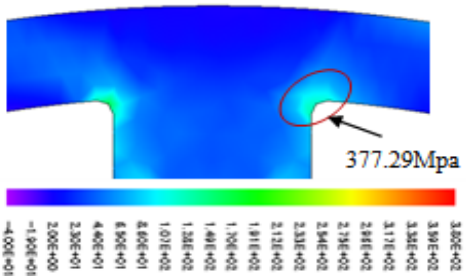

Figure-15. Principle stress distributions.

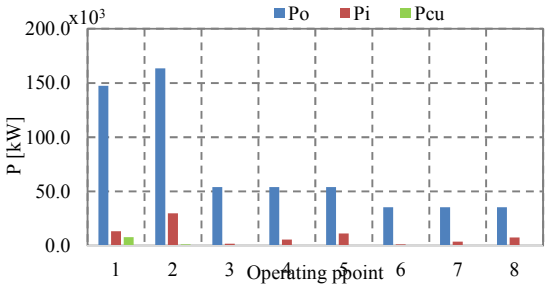

Figure-16. Output power and power loss.

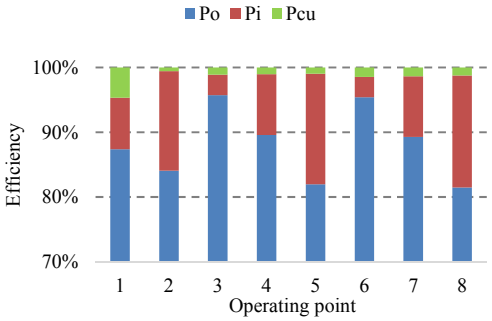

Figure-17. Power losses and motor efficiency.

CONCLUSIONS

This paper has presented an investigation of optimal torque 12S-14P outer-rotor hybrid excitation flux switching machine for direct-drive EV. The optimization process to treat optimal torque has been discussed in detail. The final design machine has successfully achieved the target performances and much better than the IPMSM conventionally employed in existing HEV. The average efficiency at normal operating condition of the final design machine is approximately 88% and acceptable for direct drive application.

ACKNOWLEDGEMENT

This study was supported by Fundamental Research Grant Scheme (FRGS), Vote No. 1508, The Ministry of Education Malaysia and Office for Research, Innovation, Commercialization and Consultancy Management (ORICC), Universiti Tun Hussein Onn Malaysia, Johor.

REFERENCES

Ahmad, M. Z., Haron, Z. A., Sulaiman, E., and Kosaka, T. 2013. Impact of rotor pole number on the characteristics of outer-rotor hybrid excitation flux switching motor for in-wheel drive EV, Procedia Technology, 11, pp. 593-601.

Chan, C. C. 2007. The state of the art of electric, hybrid, and fuel cell vehicles. Proc. IEEE, 95(4), pp. 704-718.

Chen, J. T. and Zhu, Z. Q. 2010. Winding configuration and optimal stator rotor pole combination of flux-switching PM brushless machines. Transaction on Energy Conversion, IEEE, Vol. 25, pp. 293-302.

Fei, W., Chi, K., Luk, C. K., Shen, J. X., Wang, Y. and Jin, M. 2012. A Novel Permanent-Magnet Flux Switching Machine With an Outer-Rotor Configuration for In-Wheel Light Traction Applications. Transactions on Industry Applications, IEEE, 48(5), pp. 1496–1506.

Galea, M., Gerada, C. and Hamiti, T. 2012. Design consideration for an outer rotor, field wound, flux switching machine. International Conference on Electrical Machines (ICEMS), pp. 171-176.

Pollock, C. and Brackley, M. 2003. Comparison of the acoustic noise of flux-switching and switched reluctance drive. Transaction on. Industrial Applications, IEEE, 39(3), pp. 826-834.

Pollock, H., Pollock, C., Walter, R. T. and Gorti, B. V. 2003. Low cost high power density, flux switching machines and drives for power tools. Industry Applications Soc. Annu. Meeting, IEEE, pp. 1451-1457.

Shakila Banu, A., and RSD Wahidabanu. 2014. Performance analysis of an interior permanent magnet synchronous motor using brain emotional learning based intelligent controller. ARPN Journal of Engineering and Apllied Sciences, 7(12), pp. 2816-2822.

Sulaiman, E., Kosaka, T. and Matsui, N. 2010. Design and performance of 6-slot 5-pole PMFSM with Hybrid Excitation for hybrid electric vehicle applications. Int. Power Electronics Conference, IEEE, pp. 1962-1968.

Sulaiman, E. Kosaka, T. and Matsui, N. 2011. High power density design of 6slot-8pole hybrid excitation flux switching machine for hybrid electric vehicles. Transaction on Magnetics, IEEE, 47(10), pp. 4453-4456.

Sulaiman, E., Kosaka, T. and Matsui, N. 2014. Design and analysis of high-power/high-torque density dual excitation switched-flux machine for traction drive in HEVs. Renewable and Sustainable Energy Reviews, Vol. 34, pp. 517-524.

Tang, Y., Paulides, J .J. H., Motoasca, T. E. and Lomonova, E.A. 2012. Flux-switching machine with DC excitation. Transaction on Magnetics, IEEE, 48(11), pp. 3583-3586.

Wang, Y. and Deng, Z. 2012. Comparison of hybrid excitation topologies for flux-switching machines. Transaction on Magnetics, IEEE, 48(9), pp. 2518-2527.

Xu, W., Zhu, J., Zhang, Y., Wang, Y., Li, Y. and Hu, J. 2010. Flux-switching permanent magnet machine drive system for plug-in hybrid electrical vehicle. Conference on Australian Universities Power Engineering (AUPEC), IEEE, pp. 1-6.

Xu, Y., Li, Q. Z., Zhang, L. and Ma, Q. 2009. Development of permanent magnet synchronous motor for electric vehicle. Conference on Sustainable Power Generation and Supply, pp. 1-5.

Yan, J. H., Lin, H., Feng, Y., Zhu, Z. Q., Jin, P., and Guo, Y. J. 2013. Cogging torque optimization of flux-switching transverse flux permanent magnet machine. IEEE Trans. Magn. 49(5), pp. 2169-2172.